ISSN 2004-2965 Energy Proceedings, Vol. 23, 2021

International Conference on Applied Energy 2021
Nov. 29 - Dec. 5, 2021, Thailand/Virtual
Paper ID: 294

A first parameterization of the pore-structure dependent kinetic adsorption model for O_2 adsorption in biomass conversion modeling

Carsten Wedler[1,2], Tim Eisenbach[1], Jannik Schwarz[1], Roland Span[1]

[1] Thermodynamics, Ruhr University Bochum, 44780 Bochum, Germany

[2] Department of Chemical Engineering, Imperial College London, London, SW7 2AZ, UK

ABSTRACT

Mass transport properties of the oxidation and gasification agents O_2, CO_2, and H_2O are highly relevant for the modeling of the conversion process of biomasses. Therefore, this study presents experimental investigations on the adsorption kinetics of O_2 on a biomass char using a modified gravimetric sorption device. Based on this comprehensive set of adsorption kinetic data, a first parameterization of the pore-structure dependent kinetic adsorption (PSK) model for O_2 adsorption is presented. This model intends to account for mass transport during biomass conversion in a more meaningful way as it is considered in conventional conversion models. With this parameterization, the model is capable of describing accurately the adsorption kinetics of O_2 as a function of time, temperature, and pressure.

Keywords: Biomass conversion, mass transport, adsorption kinetics, oxygen, pore-structure dependent adsorption kinetic model.

NOMENCLATURE

EOS	Equation of state
HTC	Hydrothermal carbonization
mi	Micropores
mm	Meso- to macropores
NLDFT	Nonlocal density functional theory
PSK	Pore-structure dependent kinetic adsorption
ul	Ultramicropores
a	Kinetic time constant
A	Surface area
c	Thickness of sorption layer
H	Heat of adsorption
k	Pressure dependence
n	Kinetic temperature dependence
m_{01}	Lifted mass
m_{ads}	Adsorbed mass
m_s	Sample mass
M	Molecular mass
p	Pressure
q	Adsorbed loading
R	Molar gas constant
t	Time
T	Temperature
V_{01}	Lifted volume
W_{01}	Weighing value
α	Balance calibration factor
ϕ	Coupling factor
ρ	Mass density
ρ_m	Molar density

1. INTRODUCTION

During the conversion of biomass fuels, mass transport processes play a decisive role. The gasification and combustion agents O_2, CO_2, and H_2O diffuse to the surface of the biomass particles and react with the carbon, and consequently, the resulting products have to leave the surface [1]. In the case of oxyfuel combustion, where the fuel is burnt with a mixture of O_2 and CO_2, mass transport is even more crucial as the two gases compete with each other [2]. Up to now, these mass transport processes have usually been taken into account in the modeling of the conversion process on the basis of effective diffusion coefficients [3,4]. However, on the one hand, this does not take the pore size

Selection and peer-review under responsibility of the scientific committee of the 13th Int. Conf. on Applied Energy (ICAE2021).

distribution of the fuel into account, which is particularly important in biomass combustion [5]. On the other hand, the calculation of the effective diffusion coefficient usually requires the tortuosity of the fuel [6], which is hardly accessible by experiments and is thus often estimated [2]. Moreover, the porous structure of solid fuels changes during the conversion process, which implies that the tortuosity is changing as well. This change depends on conversion temperature, heating rate, and gas atmosphere [7–10]. However, it is also possible to determine diffusion coefficients based on sorption kinetic studies [11–14]. But until recently, these sorption kinetic data could not be taken into account in conversion modeling. To integrate the data from sorption kinetic studies, a new pore-structure dependent kinetic adsorption (PSK) model was developed within the framework of the collaborative research center Oxyflame, [15]. This model is intended to provide a more meaningful consideration of mass transport processes in biomass conversion modeling. The pore structure of the biomass fuel is considered by detailed 2D nonlocal density functional theory (NLDFT) calculations, which are based on volumetric adsorption data. Based on comprehensive kinetic adsorption experiments, the PSK model allows for the determination of adsorption flow rates, mass transfer coefficients, and effective diffusion coefficients as a function of time, temperature, and pressure. This enables the calculation of meaningful time-resolved coefficients [16], which can be implemented in biomass conversion models.

The PSK model has already been validated using experiments with CO_2 [15], but studies on O_2 and H_2O are still pending. Within the scope of this study, comprehensive investigations on the adsorption kinetics of O_2 on a biomass char were carried out, and a first parameterization of the PSK model for the adsorption kinetics of O_2 was obtained. With these new data, a significant step is taken towards the meaningful description of mass transfer processes during the conversion of solid biomass fuels.

2. EXPERIMENTAL

2.1. Materials

The adsorption of O_2 was studied on a biomass char, which was derived via hydrothermal carbonization (HTC). Afterward, the HTC char was pyrolyzed in a horizontal oven using a heating rate of 5 K/min up to a temperature of 1073 K. Details on the HTC and the pyrolysis process can be found elsewhere [17,18]. The HTC char is the same sample already used for the adsorption measurements with CO_2 by Wedler and Span [15], who carried out an intensive pore surface analysis via 2D NLDFT calculations. Based on volumetric adsorption experiments with CO_2 and N_2, Wedler and Span [15] determined pore surface areas of the HTC char for different pore regimes (see Table 1): meso- to macropores (mm, $d_p > 2$ nm), micropores (mi, 2 nm > d_p > 0.7 nm), and ultramicropores (ul, $d_p < 0.7$ nm). For the adsorption studies, O_2 with a purity of 99.9992 mol-% supplied by Air Products was used.

Table 1. Values for the pore surface area of the HTC char classified into three different pore regimes: meso- to macropores (mm), micropores (mi), and ultramicropores (ul) [15].

A_{mm} [m²/g]	39.3
A_{mi} [m²/g]	225.1
A_{ul} [m²/g]	286.6

2.2. Adsorption measurements

To perform the kinetic adsorption measurements, a modified gravimetric sorption device, which is based on a magnetic suspension balance of Rubotherm (since 2016 TA Instruments), was used. The device is able to measure the difference in weight of the sample due to the adsorption of O_2; thus, the adsorbed mass of O_2, m_{ads}, can be determined. The modified device and the measurement procedure are intensively described by Wedler and Span [15]. Before a kinetic measurement was started, the HTC char in the measurement cell was degassed by evacuating the cell at a temperature of 473.15 K. The measuring cell was then cooled down to the measuring temperature and the kinetic measurement was started from the evacuated state. The pressure of O_2 in the measuring cell was instantaneously increased by opening a pneumatic valve, connected to an O_2 supply vessel. Due to the increase in pressure, the adsorption process of O_2 starts and the weighing value $W_{01}(p, T, t)$ increases with time. However, the pressure increase also leads to temporary density fluctuations in the measuring cell, resulting in the weighing signal being reliably recorded after approximately 5 seconds. The measurements were conducted at temperatures of 298 K, 323 K, 348 K, and 373 K and pressures between 30 kPa and 300 kPa.

The weighing value has to be converted to the adsorbed mass according to Eq. (1), considering the balance calibration factor α, the coupling factor ϕ, which takes the force transmission of the magnetic field into account [19], the density $\rho_{O2,EOS}$ at measuring

temperature T and pressure p, and the mass m_{01} and volume V_{01} of the lifted parts, including mass and volume of the char sample. The density of O_2 was calculated using the equation of state (EOS) by Schmidt and Wagner [20] as implemented in the software package *TREND 5.0* [21]. The values for α, ϕ, m_{01}, and V_{01} were determined as described by Rösler and Wedler [22]. By considering the sample mass m_s and the molecular mass M_{O2} of O_2, the time-dependent loading q was calculated according to Eq. (2).

$$m_{\mathrm{ads}}(p,T,t) = \frac{W_{01}(p,T,t)}{\alpha \cdot \phi\left(\rho_{\mathrm{O_2,EOS}},t\right)} - m_{01} + \rho_{\mathrm{O_2,EOS}}(T,p,t) \cdot V_{01} \quad (1)$$

$$q(p,T,t) = \frac{m_{\mathrm{ads}}(p,T,t)}{M_{\mathrm{g}} \cdot m_{\mathrm{s}}} \quad (2)$$

3. PSK MODELING

The experimental data was used to adjust the PSK model according to Eq. (3), which is able to describe the adsorption loading q as a function of pressure, temperature, and time [15]. Three identical terms describe the adsorption for the surface areas A_i of the three different pore regimes (mm, mi, and ul) separately. For each pore regime, an effective thickness of the sorption layer c_i at equilibrium state, the pressure dependence k_i at equilibrium state, the heat of adsorption H_i, the kinetic time constant a_i, and the kinetic temperature dependence n_i are adjusted to describe the experimental data. For the molar density, the critical molar density ρ_m = 13.63 kmol/m³ was considered [20]. The reference temperature T_{ref} is defined as 298.15 K [15].

$$q(t,p,T) = \rho_{\mathrm{m}} \cdot \sum_{i=1}^{3} A_{\mathrm{i}} \cdot c_{\mathrm{i}} \cdot \frac{p \cdot k_{\mathrm{i}} \cdot \mathrm{e}^{H_{\mathrm{i}}/R \cdot T}}{1 + p \cdot k_{\mathrm{i}} \cdot \mathrm{e}^{H_{\mathrm{i}}/R \cdot T}} \cdot \left(1 - \mathrm{e}^{\frac{-t}{a_i \cdot \left(\frac{T}{T_{\mathrm{ref}}}\right)^{-n_i}}}\right) \quad (3)$$

4. RESULTS

4.1. Adsorption kinetic experiments

In Figure 1, the adsorption kinetics of O_2 on the HTC char are exemplarily shown for three different pressures at an approximate temperature of 298 K. It can be seen clearly that after a few seconds the majority of the adsorption has already taken place. This is more pronounced at lower pressure than at higher pressure, which is consistent with the results for CO_2 adsorption reported by Wedler and Span [15]. However, the adsorption kinetics for O_2 are significantly faster than for CO_2. For the adsorption kinetics of O_2 at a pressure of 99 kPa, 95% of the equilibrium loading is already reached after 30 s, while for CO_2 95 % were reached after 300 s [15]. This can be explained by the significantly lower equilibrium loading and the smaller molecule size, but further studies should be performed in this regard.

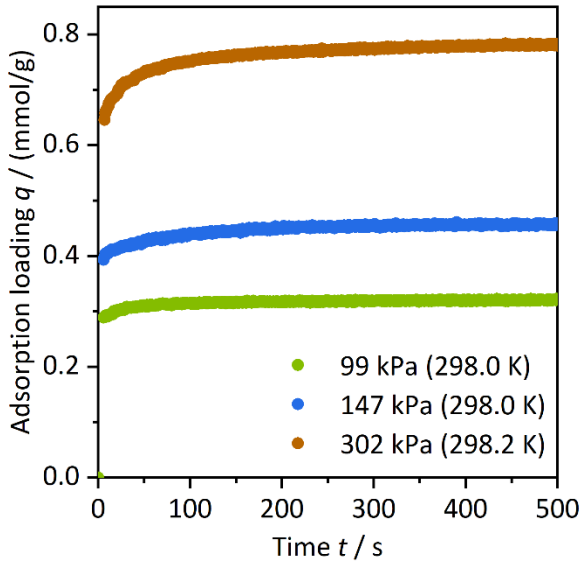

Figure 1. Adsorption kinetics of O_2 at approximately 298 K and three different pressures.

4.2. Adsorption kinetic modeling

The comprehensive experimental data set was used to adjust the PSK model and to obtain a first parametrization for O_2 (see Table 2). In Figure 2, the modeling results (black lines) for the adsorption kinetic curves at three different pressures are shown on a logarithmic time scale and are compared to the experimental data (colored symbols). It can be seen that the PSK model with this parametrization can already describe the experimental adsorption curve accurately. Furthermore, the advantage of the time-dependent modeling becomes apparent, since reasonable kinetic curves can also be obtained for the time periods below 5 seconds, for which no experimental data could be recorded. The slightly fluctuating course of the modeled curves can be explained by the fact that the experimentally measured values for temperature and pressure were used for modeling.

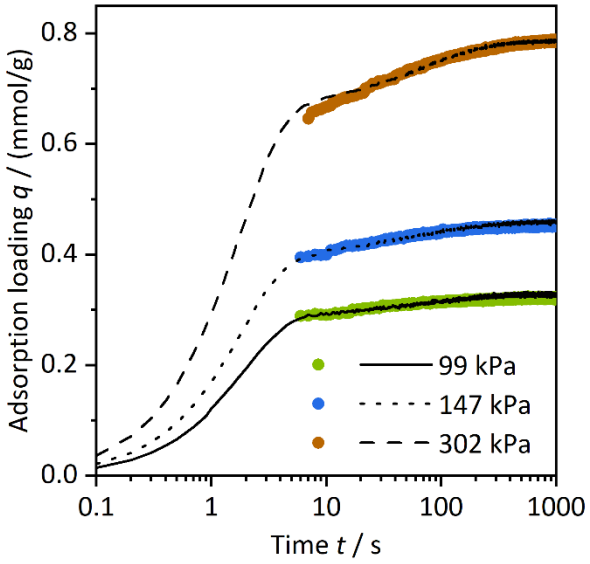

Figure 2. Results of the PSK modeling (black lines) at approximately 298 K and three different pressures compared with the experimental values (colored symbols).

By comparing the parameters in Table 2, it can be concluded that this is only a preliminary parameterization and should be further optimized. For example, the value for the exponent *n* describing the temperature dependence of the kinetics in the micropores is significantly higher than for the other two pore regimes, which does not represent a reasonable temperature dependency for the exponential term in Eq. (3). This can also be confirmed by comparison with the parameters obtained by Wedler and Span [15] for CO_2. The same applies to the average thickness of the sorption layers in the micropores, as this value appears to be too small compared to the other pore regimes.

Table 2. Preliminary parametrization of the PSK model for the adsorption kinetics of O_2 on the HTC char

	mm	mi	ul
c_i [nm]	4.203	0.052	0.094
k_i [1/kPa]	$9.16 \cdot 10^{-7}$	$9.15 \cdot 10^{-7}$	$9.64 \cdot 10^{-6}$
H_i [kJ/mol]	18.44	18.64	6.15
a_i [s]	1.888	104.6	303.2
n_i [-]	3.775	28.52	2.767

5. CONCLUSION

The presented measurement results for O_2 adsorption on a biomass char indicate very fast adsorption kinetics compared to CO_2. With the parametrization obtained within this study, the PSK model is capable of describing the course of the adsorption kinetic curves accurately. These new data are an important contribution towards a more meaningful description of mass transfer processes during the conversion of solid biomass fuels. However, it is obvious that this should only be a preliminary parameterization since some parameters seem to be physically unreasonable. Although the kinetic curves can be described well, there will be problems with a further interpretation of the data. If the parameterization would be used for the determination of adsorption flows rates, effective diffusion coefficients, or mass transfer coefficients, it can be assumed that these values would not be meaningful. In order to obtain reasonable values for the modeling of conversion processes, the parameterization must be optimized. The further improvement of the parameterization considering all our underlying data for O_2 adsorption is part of ongoing studies.

ACKNOWLEDGEMENT

This work has been funded by the Deutsche Forschungsgemeinschaft (DFG, German Research Foundation) – Projektnummer 215035359 – TRR 129.

REFERENCES

[1] Van de steene L, Tagutchou JP, Escudero Sanz FJ, Salvador S. Gasification of woodchip particles: Experimental and numerical study of char–H_2O, char–CO_2, and char–O_2 reactions. Chemical Engineering Science 2011;66(20):4499–509. https://doi.org/10.1016/j.ces.2011.05.045.

[2] Ollero P, Serrera A, Arjona R, Alcantarilla S. Diffusional effects in TGA gasification experiments for kinetic determination. Fuel 2002;81(15):1989–2000. https://doi.org/10.1016/S0016-2361(02)00126-6.

[3] Holland T, Fletcher TH. Comprehensive Model of Single Particle Pulverized Coal Combustion Extended to Oxy-Coal Conditions. Energy Fuels 2017;31(3):2722–39. https://doi.org/10.1021/acs.energyfuels.6b03387.

[4] Jeong HJ, Seo DK, Hwang J. CFD modeling for coal size effect on coal gasification in a two-stage commercial entrained-bed gasifier with an improved char gasification model. Appl. Energy 2014;123:29–36. https://doi.org/10.1016/j.apenergy.2014.02.026.

[5] Fatehi H, Bai X-S. Structural evolution of biomass char and its effect on the gasification rate. Appl. Energy 2017;185:998–1006. https://doi.org/10.1016/j.apenergy.2015.12.093.

[6] Wedler C, Richter M, Span R. Integration of sorption kinetics in carbon conversion modeling for the description of oxyfuel combustion processes. Energy Procedia 2017;142:1361–6. https://doi.org/10.1016/j.egypro.2017.12.520.
[7] Vyas A, Chellappa T, Goldfarb JL. Porosity development and reactivity changes of coal–biomass blends during co-pyrolysis at various temperatures. Journal of Analytical and Applied Pyrolysis 2017;124:79–88. https://doi.org/10.1016/j.jaap.2017.02.018.
[8] Fu P, Hu S, Xiang J, Sun L, Su S, Wang J. Evaluation of the porous structure development of chars from pyrolysis of rice straw: Effects of pyrolysis temperature and heating rate. Journal of Analytical and Applied Pyrolysis 2012;98:177–83. https://doi.org/10.1016/j.jaap.2012.08.005.
[9] Yuan S, Chen X, Li J, Wang F. CO_2 Gasification Kinetics of Biomass Char Derived from High-Temperature Rapid Pyrolysis. Energy Fuels 2011;25(5):2314–21. https://doi.org/10.1021/ef200051z.
[10] Wedler C, Span R, Richter M. Comparison of micro- and macropore evolution of coal char during pyrolysis. Fuel 2020;275:117845. https://doi.org/10.1016/j.fuel.2020.117845.
[11] Pillalamarry M, Harpalani S, Liu S. Gas diffusion behavior of coal and its impact on production from coalbed methane reservoirs. International Journal of Coal Geology 2011;86(4):342–8. https://doi.org/10.1016/j.coal.2011.03.007.
[12] Charrière D, Pokryszka Z, Behra P. Effect of pressure and temperature on diffusion of CO_2 and CH_4 into coal from the Lorraine basin (France). International Journal of Coal Geology 2010;81(4):373–80. https://doi.org/10.1016/j.coal.2009.03.007.
[13] Wedler C, Arami-Niya A, Xiao G, Span R, May EF, Richter M. Sorption Kinetics of CO_2, CH_4 and O_2 on Cellulose-based Hydrochars for Carbon Conversion Modelling. In: Thermodynamik-Kolloquium 2018; 2018.
[14] Seibel C, Wedler C, Vorobiev N, Schiemann M, Scherer V, Span R et al. Sorption measurements for determining surface effects and structure of solid fuels. Fuel Process. Technol. 2016;153:81–6. https://doi.org/10.1016/j.fuproc.2016.08.004.
[15] Wedler C, Span R. A pore-structure dependent kinetic adsorption model for consideration in char conversion – Adsorption kinetics of CO_2 on biomass chars. Chemical Engineering Science 2021;231:116281. https://doi.org/10.1016/j.ces.2020.116281.
[16] Wedler C. Investigations on adsorption processes and pore structure development during solid fuel conversion. Dissertation. Ruhr-Universität Bochum. Bochum; 2020. https://doi.org/10.13154/294-7724.
[17] Wedler C, Lotz K, Arami-Niya A, Xiao G, Span R, Muhler M et al. Influence of Mineral Composition of Chars Derived by Hydrothermal Carbonization on Sorption Behavior of CO_2, CH_4, and O_2. ACS Omega 2020;5(19):10704–14. https://doi.org/10.1021/acsomega.9b04370.
[18] Lotz K, Wütscher A, Düdder H, Berger CM, Russo C, Mukherjee K et al. Tuning the Properties of Iron-Doped Porous Graphitic Carbon Synthesized by Hydrothermal Carbonization of Cellulose and Subsequent Pyrolysis. ACS Omega 2019;4(2):4448–60. https://doi.org/10.1021/acsomega.8b03369.
[19] Kleinrahm R, Yang X, McLinden MO, Richter M. Analysis of the systematic force-transmission error of the magnetic-suspension coupling in single-sinker densimeters and commercial gravimetric sorption analyzers. Adsorption 2019;25(4):717–35. https://doi.org/10.1007/s10450-019-00071-z.
[20] Schmidt R, Wagner W. A new form of the equation of state for pure substances and its application to oxygen. Fluid Phase Equilibria 1985;19(3):175–200. https://doi.org/10.1016/0378-3812(85)87016-3.
[21] Span R, Beckmüller R, Hielscher S, Jäger A, Mickoleit E, Neumann T et al. TREND. Thermodynamic Reference and Engineering Data 5.0: Software: Lehrstuhl für Thermodynamik, Ruhr-Universität Bochum; 2020.
[22] Rösler M, Wedler C. Adsorption kinetics and equilibria of two methanol samples with different water content on activated carbon. Adsorption 2021. https://doi.org/10.1007/s10450-021-00341-9.

